DOI: 10.1002/adma.200600475

Synthesis and Optical Properties of Gold Nanodecahedra with Size Control**

By *Ana Sánchez-Iglesias*, *Isabel Pastoriza-Santos*, *Jorge Pérez-Juste*, *Benito Rodríguez-González*, *F. Javier García de Abajo*, and *Luis M. Liz-Marzán**

The synthesis of nanoparticles with a tight control on their size and shape is a requirement for the achievement of many nanotechnology goals, since these are the main parameters determining the material properties at the nanoscale. Among the many different materials currently under investigation, semiconductor and metal nanoparticles are extremely attractive because of the possibility of controlling their electronic and optical properties through tailoring size and shape during synthesis. For instance, the presence of sharp edges or tips has been shown to increase electric-field enhancement,[1] which is important for applications involving metal nanoparticles as sensors. Additionally, nanoparticle morphology will ultimately determine the way in which nanoparticles can be assembled.

While spheres, rods, cubes, and flat prisms are the most thoroughly studied shapes, there have been several reports on the synthesis and detailed characterization of other geometries, and it is believed that metal nanoparticles tend to grow with the structure of one of the Platonic solids, that is, with all faces made of the same regular polygon and the same number of polygons meeting at each corner.[2–4] Non-Platonic structures that have been reported for metal nanocrystals include nanorods, either with the geometry of single-crystal or penta-twinned prisms,[5–9] as well as flat platelets, usually with triangular or hexagonal shape,[10–13] in which faces are made of more than one polygon. Recently, other elaborate geometries have also been reported, such as nanocages[14] or nanostars.[15] In this paper we report the synthesis with tight size control and high monodispersity of nanometer-sized, uniform gold nanoparticles with decahedral morphology, in which all ten faces are equilateral triangles, but not the same number of triangles meet at every corner (four or five are possible), and for this reason they do not qualify as Platonic nanocrystals, but can rather be classified as Johnson structures. These decahedral particles have a lower symmetry (D_{5h}) than Platonic solids, but still display a striking beauty and attractive optical properties that are strongly influenced by particle size. Although the geometry (and thus the aspect ratio) is precisely the same for particles with different sizes, clear changes in the optical responses have been observed and modeled through a boundary element method (BEM) for bicones.

The synthesis is based on our previous work where *N*,*N*-dimethylformamide (DMF) was used as both solvent and reducing agent[16] to generate silver nanoparticles of various shapes, including spheres,[17] nanoprisms[18] and nanowires.[19] The synthesis of gold nanoparticles with this system had been rather elusive, though Lofton et al. reported a variation of the method for making gold nanoprisms,[13] and Chen et al. reported formation of large particles with various shapes.[20] In an attempt to follow a more controlled procedure, we carried out the reduction of $HAuCl_4$ using DMF in the presence of small (2–3 nm) gold seeds with uniform size distribution, presynthesized following a procedure reported by Teranishi et al.,[21] using $NaBH_4$ as a strong reducing agent and poly(vinylpyrrolidone) as a stabilizer. Even though the presence of the seeds was expected to assist gold reduction, with the gold surface acting as a catalyst, the thermal reduction at reflux produced a lower yield of decahedra, with a noticeable polydispersity and presence of other less-defined geometries in all samples. We found that the use of ultrasound (see Experimental) was a key step to the controlled and reproducible synthesis of monodisperse decahedra with high yield. During sonication, spectacular color changes can be seen, ranging from light red to deep blue through a variety of purple and violet tones, as shown in Figure 1 (top). Ultrasound has been previously used for metal-nanoparticle synthesis,[22–29] based on the effects derived from acoustic cavitation, such as the ability to induce the formation of radicals, though we believe that the main effect of ultrasound here is a noticeable temperature increase (up to 100 °C). Experiments carried out with ultrasound irradiation but limiting temperature by means of a thermostating bath did not result in growth of decahedra, which is in accordance with a related report by Li et al.[30] When the so-prepared samples were examined using transmission electron microscopy (TEM), it was found that a large proportion of the particles had an extremely regular pentagonal symmetry. As can be readily observed in Figure 1, the yield of such

[*] Prof. L. M. Liz-Marzán, A. Sánchez-Iglesias, Dr. I. Pastoriza-Santos, Dr. J. Pérez-Juste, Dr. B. Rodríguez-Fernández
Departamento de Química Física and Unidad Asociada CSIC
Universidade de Vigo
36310 Vigo (Spain)
E-mail: lmarzan@uvigo.es
Dr. F. J. García de Abajo
Centro Mixto CSIC-UPV/EHU and
Donostia International Physics Center
Apartado 1072, 20080 San Sebastián (Spain)

[**] This work has been supported by the Spanish Ministerio de Educación y Ciencia, through Grants No. MAT2003-02991 and NAN2004-08843-C05-03(05). Supporting Information is available online from Wiley InterScience or from the author.

ADVANCED MATERIALS

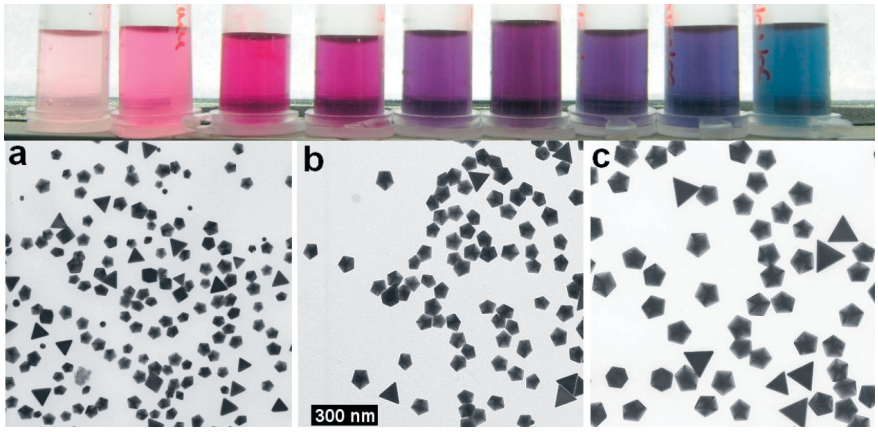

Figure 1. Top: photograph of samples withdrawn from the reacting solution at various times during a typical synthesis. Bottom: TEM images of decahedral gold nanoparticles prepared by sonication (60 min) using different amounts of gold-seed solution (a: 1.4 mL, b: 0.7 mL, c: 0.3 mL). The scale is the same in all TEM images.

pentagonal shape is very high (typically around 80–90 %), with most of the remaining particles having the shape of triangular prisms. It should also be noted that the final particle size is mainly determined by the initial ratio between the amount of gold seed present and $HAuCl_4$ concentration, which allows easy size tuning, and that the monodispersity was in most experiments as high as 10 %.

Although it was clear from the start that the pentagonal symmetry was dominating and fivefold twinning was apparent on most particles, the precise morphology could not be completely discerned using standard TEM. To obtain a clear picture, it was necessary to carry out tilting experiments, so that the lateral shape could be observed. Since various orientations were present within each TEM grid preparation, and the maximum tilting angles allowed by our instrument were ±45°, particles were searched that allowed a complete 90° tilt from perpendicular view to parallel view, so that a full picture of the geometry could be obtained. A representative example is shown in Figure 2, but the results were confirmed with other particles. The observation was always performed on the same particle for the different tilting angles, and we invariably obtained clear evidence that the particles were nearly perfect pentagonal bipyramids of equal equilateral-triangle faces, but with somewhat rounded edges. The dimensions measured for the particle shown in Figure 2 are: side length $e = 44$ nm, height (distance from the pentagon to the central tip) $h = 23$ nm, with an aspect ratio that agrees with the geometrical relationship for a regular pentagonal bipyramid

$$(h = \tfrac{1}{10}\sqrt{50 - 10\sqrt{5}}e) \qquad (1)$$

The same ratio was found for other particles studied.

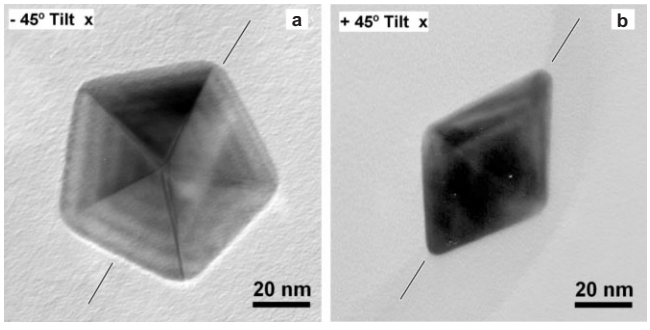

Figure 2. TEM images of the same particles as in Figure 1. Top and lateral views were obtained by using ±45° tilting angles. A pentagonal bipyramid geometry is evidenced. The lines are an indication of the rotation axis.

The high-magnification image shown in Figure 2a reveals again the presence of fivefold twinning from the center of the particle, and there seems to be inhomogeneous broadening of some twin boundaries near the tip. Similar broadening has been previously reported to describe the structure of gold[6] and silver[7,31] nanowires with pentagonal cross section and it stems from the deviation of the angle of a perfect twin in gold {111} faces (70.53°) from 360°/5 (72°). The presence of dislocations has been predicted as a means to adjust the lattice mismatch, but it has not been clearly reported before.

The regular structure of these particles was further demonstrated using high-resolution TEM (HRTEM) observation at various sections within single particles. We found in all cases that each of the twins displays single-crystal structure, with well-defined intersections, which can be easily assigned to twin boundaries. In Figure 3a, a HRTEM image of the center of a decahedron is shown. The image was obtained in the [110] zone axis, so that the five twin zones were visible, as well as twin planes, and the twin axis was precisely located in the center. Shown in Figure 3b is another HRTEM image taken at one edge, in which no dislocations are observed, apart from just a slight distortion at the twin plane. We also obtained the selected-area electron diffraction (SAED) pattern (Fig. 3c) from single particles. In the image, the spots for (00–2) reflections from each twin (T1–T5) are indicated with solid circles, demonstrating a pseudo fivefold axis symmetry. The dashed circles show the various fcc reflections for T1 in a [110] zone axis, and it has been confirmed that rotation by 72° yields the reflections for all subsequent twins. The diffraction pattern also shows streaks between some spots, which are characteristic of diffraction from areas containing twin planes.[32]

The optical properties of these decahedra, arising from surface-plasmon resonances, could be in principle expected to agree reasonably well with those of oblate ellipsoids, which can be modeled using Mie–Gans equations,[33] widely used to simulate the optical response of small metal particles. However, there are obvious geometrical differences, since the

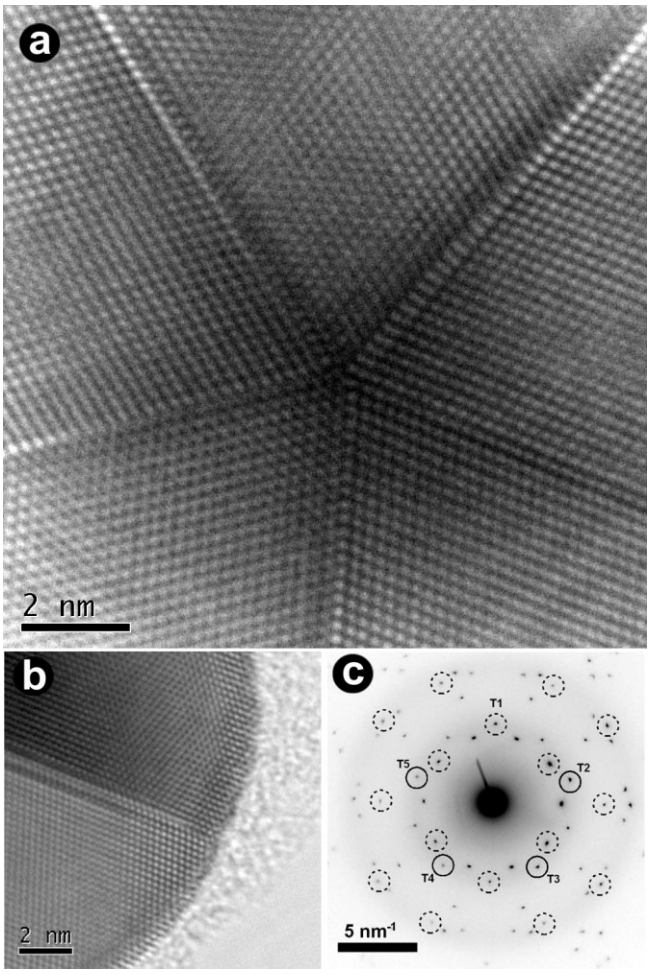

Figure 3. a,b) HRTEM images from the center (a) and an edge (b) of a gold nanodecahedron, clearly showing the presence of five twin planes, necessary to achieve fivefold symmetry with angles of 72°. c) Electron-diffraction pattern obtained at the center of a particle. The (00–2) reflections of each twin are marked with solid circles, while dashed circles indicate the reflections from twin T1.

pentagonal bipyramid has not only pentagonal rather than circular section, but also has much shaper edges than those of an oblate ellipsoid. Additionally, Mie–Gans theory only accounts for particle size through the volume, and we found that for the sizes we deal with here the position of the main absorption band would only shift marginally, while experimentally we find red-shifts of ca. 60 nm when the pentagon edge length is increased from 36.5 to 64.5 nm (see Fig. 4). For this reason, it was necessary to carry out more sophisticated theoretical modeling, by calculating total extinction cross sections via the optical theorem[34] for an incident plane wave. Since the experiments probe a large number of particles in solution with random orientations with respect to the incoming light, calculated total cross sections were averaged over all possible orientations of the particles and polarizations of the incident beam. The optical theorem relies on the far-field forward scattering amplitude, which we calculated by means of the boundary element method.[35,36] In the BEM the induced electric and magnetic fields are viewed as originating from equivalent boundary sources (i.e., equivalent surface electric charges and currents), which are used to fulfill the customary boundary conditions at the interfaces between different media. The number of boundary elements increases quadratically with the size of the particle, as compared to the cubic increase in volume elements required by other approaches such as the discrete-dipole approximation (DDA),[37] which makes the BEM more computationally economical. Further details on the calculation method are provided in the Experimental section. Since the BEM works particularly well for axially symmetric shapes, we modeled our pentagonal bipyramids by means of bicones (of height h and radius r), as schematically shown in the inset of Figure 4, lower-left plot. The circular edge and the tips of the cones were rounded with radii of curvature of 2 nm, in order to avoid sharp corners that can cause numerical problems.[38] This is fully justified when we examine the geometry of the tilted bipyramid in Figure 2 and the high-resolution image in Figure 3b. Convergence has been achieved through a parametrization using 150 points. By using the BEM with the (rounded) bicone geometry, excellent agreement with the experimental results was obtained, as can be clearly seen in Figure 4. In both cases, there is a red-shift and broadening of the main plasmon band as the particle size is increased, but also a second mode becomes more and more apparent. Calculations (not shown) of the spectra with polarization at 0° and 90° with respect to the plane of the pentagon base clearly reveal that for any of these sizes there are two distinct modes (azimuthal and polar) but the relative intensity of the transverse, polar mode (at lower wavelengths) decreases for smaller particles. The noted red-shift comes from retardation effects, since the electromagnetic interaction between charges and currents induced on opposite regions of the particle surface undergoes a phase shift that is proportional to the ratio of the particle size to the wavelength, which can be quantified as 40–85° for the particle dimensions under consideration. Simultaneously, the induced dipole increases with particle size and so does its coupling to free light, causing radiative broadening both in experiment and theory.

All these results confirm that the choice of the bicone geometry to model the bipyramids is appropriate (BEM calculations for oblate ellipsoids yielded a similar agreement in the trend, but with considerable blue-shifts of the peak positions) and allows predicting the optical response of decahedra of various sizes. We should, however, point out that the degree of curvature assigned to the edges and tips of the bicone has a noticeable influence on the actual maximum position, indicating the large effect of sharp edges on field enhancement, which has been reported for the tips of triangular prisms,[1] and can be important in potential applications in surface-enhanced Raman spectroscopy (SERS) and biosensing. Preliminary calculations of the near-field enhancement were carried out using the BEM and confirm large enhancements at the tips (for the polar mode) and at the edges (for the azimuthal mode), as shown in Figure 4. Near-field enhancement maps for the other two samples are shown in the Supporting Infor-

ADVANCED MATERIALS

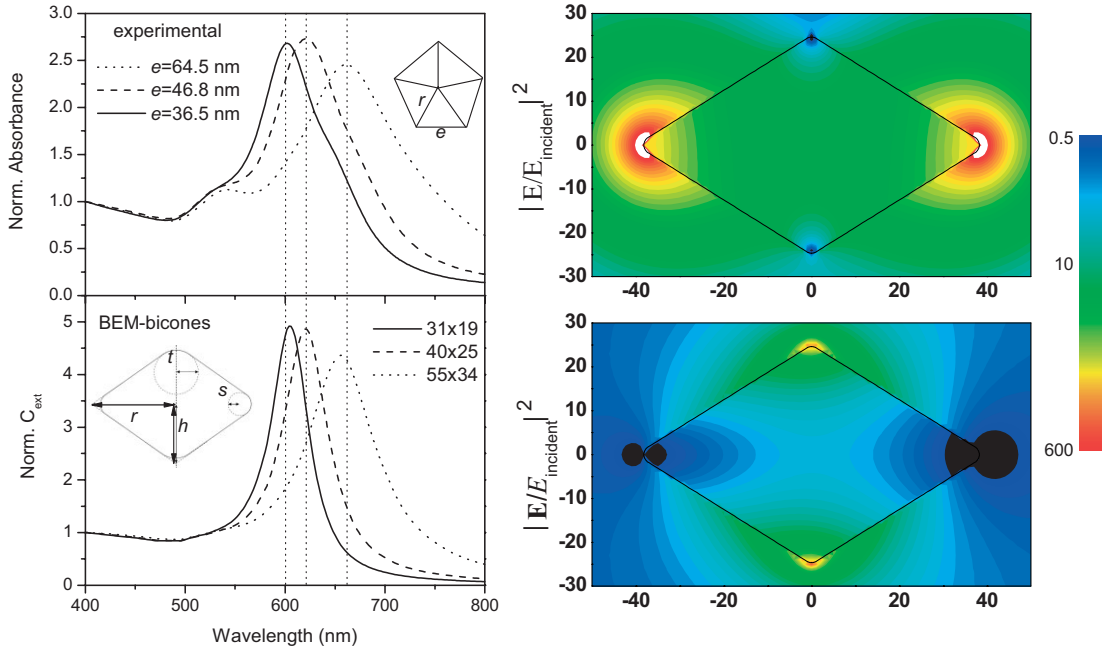

Figure 4. Left: UV-vis spectra of flattened gold nanoparticles. The upper plot contains experimental spectra for nanodecahedra samples with different average particle size (e = pentagon side length). The bottom plot shows calculated spectra using the boundary elements method for bicones with radius r and height h, as indicated. Edge curvature was included with $s = t = 2$ nm (see drawing). All spectra were normalized at 400 nm. Right: plots of the calculated near-field enhancement ($|E/E_{incident}|^2$) for bicones with 40 nm radius and 25 nm height in the azimuthal (top, incident field along the horizontal symmetry plane) and polar (bottom, incident field along the symmetry axis) modes. Light is coming from below in the upper plot and from the left in the lower one, with the electric field contained in the plane of the plots. For the calculations, the wavelengths of maximum extinction cross section (620 and 522 nm, respectively) were used. The vertical and horizontal axes are in nanometers.

mation (Fig. S1). Finally, we observe that the experimental spectra are wider than the calculated ones, which is likely to arise from a certain polydispersity (around 10 %) observed experimentally.

The formation of nanoparticles with such a regular fivefold symmetry appears to be related to the structure of the small seeds used, which have been repeatedly reported to display fivefold twinning.[3] This initial crystalline structure is likely to influence the way in which the final particles grow, as has been reported for nanorods.[26] In the process reported here, the role of the ultrasonic treatment is on the one hand related to a continuous supply of the energy needed for reduction of the Au^{III} salt, and on the other hand to a most uniform approach of ions to all faces of the seeds, so that the growth takes place on each face simultaneously. Evidence for this has been found from the fact that the decahedral geometry is characteristic of most of the particles from early stages of the reaction, and the particle size steadily increases as the reaction proceeds. Additionally, we have used preformed decahedral nanoparticles as seeds for further growth using the same procedure, invariably observing that the characteristic decahedral geometry is maintained, but the nanoparticles grow steadily, as shown in the Supporting Information (Fig. S2).

The final piece of evidence in favor of the proposed growth mechanism is provided by a complementary experiment in which single-crystal seeds are used, which, following the same argument, should induce the formation of larger, single-crystal particles. The experiment was carried out using platinum nanoparticles (2–3 nm) as seeds for the growth of gold on them. These platinum nanoparticles have been reported by various groups[39,40] to display predominantly a single-crystal structure (which we have confirmed, data not shown), initially with tetrahedral symmetry but becoming octahedra or truncated octahedra upon further growth. The ultrasound-induced reduction of $HAuCl_4$ on these seeds yielded a rather different morphology than before, as shown in Figure 5. Most particles are single-crystalline octahedra as indicated by the complete absence of twin boundaries in the TEM images. The tilting and diffraction experiments shown in Figure 5 invariably point toward an almost perfect octahedral geometry (see sketch). Again, the size of the particles is very uniform and can be easily controlled through the irradiation time or the gold-salt concentration. Analysis of the SAED pattern shown in Figure 5 shows that the particle shown was oriented in the [111] zone axis, which implies that all the facets of the octahedron are of the {111} family. The absence of additional spots, apart from those expected for single-crystal gold in the [111] zone axis demonstrates the single-crystal structure of these particles.

In summary, a new class of extremely regular gold nanocrystals—decahedra (pentagonal bipyramids)—has been obtained in high yield through ultrasound-induced reduction of $HAuCl_4$ on presynthesized gold seeds, using poly(vinylpyrrolidone) (PVP) as a stabilizing polymer. The dimensions can be

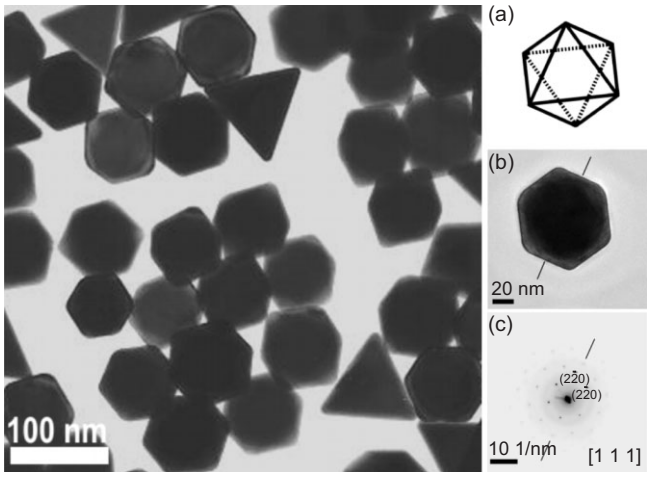

Figure 5. Representative TEM images of gold octahedra grown from single-crystal platinum seeds. SAED patterns from single particles with different orientation confirm the octahedral geometry.

controlled through the ratio between the amount of seed and the $HAuCl_4$ concentration, and the monodispersity is as good as 10 %. Additionally, we have shown that a model for the resolution of Maxwell's equations for bicones describes extremely well the optical properties of these bipyramids, so that a good correlation between particle size and optical response can be established, which will be extremely helpful to predict the optical response in biosensing applications. The relationship between the final morphology and the crystalline structure of the seeds was demonstrated through the growth on single-crystal platinum nanoparticles, producing uniform, single-crystal octahedra.

Experimental

Seed gold nanoparticles 2–3 nm in size were prepared following a procedure previously reported by Teranishi et al. [21]. Briefly, 22 μL of an aqueous solution of 0.1136 M $HAuCl_4$ (Aldrich) was added to 47.5 mL of a solution in a H_2O–DMF (Fluka) mixture (1:18; v/v) containing 0.017 g of PVP (weight-average molecular weight (M_w) = 10 000, Fluka). Next, 2.5 mL of a freshly prepared 10 mM $NaBH_4$ (Aldrich) solution was injected quickly into the solution under vigorous stirring. The gold sol was stirred for 2 h at room temperature. The seed was not used until 24 h after preparation to allow for complete $NaBH_4$ decomposition and avoid further nucleation. Seed platinum nanoparticles 2–3 nm in size were prepared following a procedure previously reported [39]. Briefly, 5 mL of an aqueous solution of 6 mM H_2PtCl_6 (Aldrich) was added to 45 mL of a solution in an ethanol–water mixture (9:1; v/v) containing 0.1332 g of PVP (M_w = 40 000, Fluka). The mixture was refluxed for 3 h under air.

Prior to seed addition, 0.825 mL of a 0.1136 M $HAuCl_4$ aqueous solution was added to 15 mL of a PVP (M_w 40 000) 2.5 mM solution in DMF in a 50 mL vessel and the mixture was ultrasonically irradiated until complete disappearance of the Au^{3+} CTTS absorption band at 325 nm. The preformed seed solution ([Au] = 5×10^{-5} M, [Pt] = 6×10^{-4} M) was then added and further ultrasonic irradiation was allowed until complete reduction, indicated by no further red-shift of the plasmon band. In the case of the experiments with gold seeds the amount of seed solution was varied between 0.3 and 1.4 mL, while for the experiment with platinum seeds 55 μL of the seed solution was added.

Ultrasonic irradiation was performed with a Sonopuls HD2200 ultrasonic horn (6.35 mm tip radius) homogenizer operating at a frequency of 20 kHz and at 30 % of the maximum power (200 W). During the reaction the DMF solution temperature was measured to be ca. 100 °C.

Optical characterization was carried out by UV-vis–near-IR spectroscopy on a Cary 5000 UV-vis–near-IR spectrophotometer, using 1 mm path length quartz cuvettes, upon 10× dilution with DMF. TEM images were obtained with a JEOL JEM 1010 transmission electron microscope operating at an acceleration voltage of 100 kV, while HRTEM studies were performed with a JEOL JEM 2010 FEG-TEM operating at an acceleration voltage of 200 kV. Samples for TEM were centrifuged at 2000 rpm and redispersed in ethanol to avoid the dissolution of the formvar polymer layer on the TEM grid by DMF and to decrease PVP concentration for increased contrast. Tilting experiments were carried out in a PHILIPS CM20 transmission electron microscope operating at 200 kV, equipped with a two-tilt axis goniometer. A grid with holey formvar film was used to find particles with suitable orientation.

Simulation of optical spectra was based on the BEM. In the BEM, scalar and vector potentials, ϕ and $\mathbf{A}$, are used and they are expressed inside each homogeneous region of space (e.g., region j) as the sum of an external field contribution (i.e., the potentials corresponding to the incident light plane wave, for which the scalar potential can be chosen as zero) and surface integrals involving the noted equivalent surface charges σ_j and currents $\boldsymbol{h}_j$, defined on the boundary of region j, S_j. In our case, $j = 1$ and 2 label DMF (index of refraction equal to 1.4275) and gold (measured frequency-dependent dielectric function taken from the literature [41], respectively. For $\mathbf{r}$ inside medium j, one has

$$\phi(\mathbf{r}) = \int_{S_j} dsG_j(|\mathbf{r} - \mathbf{s}|)\sigma_j(\mathrm{s}) \tag{2}$$

and

$$\mathbf{A}(\mathbf{r}) = \mathbf{A}^{\mathrm{ext}}(\mathbf{r}) + \int_{S_j} dsG_j(|\mathbf{r} - \mathbf{s}|)\mathbf{h}_j(\mathrm{s}) \tag{3}$$

where

$$G_j(|\mathbf{r} - \mathbf{s}|) = \frac{e^{\mathrm{ikj}|\mathrm{r}-\mathrm{s}|}}{|\mathrm{r} - \mathrm{s}|} \tag{4}$$

takes care of the propagation of the electromagnetic signal in medium j;

$$k_j = (\omega/c)\sqrt{\varepsilon_j} \tag{5}$$

is the momentum of light inside medium j of dielectric function $\varepsilon_j(\omega)$; and $\mathbf{A}^{\mathrm{ext}}$ is the vector potential associated to the incoming light, which is non-vanishing only for $j = 1$ (i.e., in the medium outside the particle). The boundary conditions of the electromagnetic field are then imposed and yield a set of self-consistent surface-integral equations that determine the surface sources and that are solved by discretizing the boundaries through a finite number of representative boundary points. This leads to a linear set of equations that is solved by linear algebra techniques [35,36]. The particles were described by axially symmetric shapes capturing the main physical aspects of their response to external illumination. The BEM is particularly advantageous in axial symmetry, where each azimuthal component m that depends on the azimuthal angle ϕ as $e^{im\phi}$ is uncoupled from the rest of the components. Then, the surface of the particle can be parametrized with a contour line, thus reducing the problem effectively to one dimension. We have assimilated the pentagonal bipyramids to bicones, which are formed by joining two cones of height h and radius r by their base. The circular edge of this structure and the tips of the cones are rounded with radii of curvature of 2 nm, in order to avoid sharp corners that can cause numerical problems [38]. Convergence beyond

ADVANCED MATERIALS

what can be resolved at the scale of the plots has been achieved with 150 parametrization points.

Received: March 8, 2006
Final version: April 29, 2006
Published online: September 14, 2006

[1] K. L. Kelly, E. Coronado, L. L. Zhao, G. C. Schatz, *J. Phys. Chem. B* **2003**, *107*, 668.
[2] F. Kim, S. Connor, H. Song, T. Kuykendall, P. Yang, *Angew. Chem. Int. Ed.* **2004**, *43*, 3673.
[3] J. M. Montejano-Carrizales, J. L. Rodríguez-López, U. Pal, M. Miki-Yoshida, M. José-Yacamán, *Small* **2006**, *2*, 351.
[4] A. S. Barnard, *J. Mater. Chem.* **2006**, *16*, 813.
[5] J. Pérez-Juste, I. Pastoriza-Santos, L. M. Liz-Marzán, P. Mulvaney, *Coord. Chem. Rev.* **2005**, *249*, 1870.
[6] C. J. Johnson, E. Dujardin, S. A. Davis, C. J. Murphy, S. Mann, *J. Mater. Chem.* **2002**, *12*, 1765.
[7] H. Chen, J. Wang, H. Yu, H. Yang, S. Xie, J. Li, *J. Phys. Chem. B* **2005**, *109*, 2573.
[8] Z. L. Wang, M. B. Mohamed, S. Link, M. A. El-Sayed, *Surf. Sci.* **1999**, *440*, L809.
[9] Y. G. Sun, Y. Xia, *Adv. Mater.* **2002**, *14*, 833.
[10] A. I. Kirkland, P. P. Edwards, D. A. Jefferson, D. G. Duff, *Annu. Rep. Prog. Chem. Sect. C* **1990**, *87*, 247.
[11] R. Jin, C. Y. Cao, E. Hao, G. Métraux, G. C. Schatz, C. A. Mirkin, *Nature* **2003**, *425*, 487.
[12] V. Germain, J. Li, D. Ingert, Z. L. Wang, M. P. Pileni, *J. Phys. Chem. B* **2003**, *107*, 8717.
[13] C. Lofton, W. Sigmund, *Adv. Funct. Mater.* **2005**, *15*, 1197.
[14] a) S. J. Oldenburg, R. D. Averitt, S. L. Westcott, N. J. Halas, *Chem. Phys. Lett.* **1998**, *288*, 243. b) J. Chen, F. Saeki, B. Wiley, H. Cang, M. Cobb, Z. Li, L. Au, H. Zhang, M. Kimmey, X. Li, Y. Xia, *Nano Lett.* **2005**, *5*, 473.
[15] a) M. Yamamoto, Y. Kashiwagi, T. Sakata, H. Mori, M. Nakamoto, *Chem. Mater.* **2005**, *17*, 5391. b) C. L. Nehl, H. Liao, J. H. Hafner, *Nano Lett.* **2006**, *6*, 683.
[16] I. Pastoriza-Santos, L. M. Liz-Marzán, *Langmuir* **1999**, *15*, 948.
[17] I. Pastoriza-Santos, L. M. Liz-Marzán, *Langmuir* **2002**, *18*, 2888.
[18] I. Pastoriza-Santos, L. M. Liz-Marzán, *Nano Lett.* **2002**, *2*, 903.
[19] M. Giersig, I. Pastoriza-Santos, L. M. Liz-Marzán, *J. Mater. Chem.* **2004**, *14*, 607.
[20] Y. Chen, X. Gu, C.-G. Nie, Z.-Y. Jiang, Z.-X. Xie, C.-J. Lin, *Chem. Commun.* **2005**, 4181.
[21] Y. Teranishi, I. Kiyokawa, M. Miyake, *Adv. Mater.* **1998**, *10*, 596.
[22] M. Ashokkumar, F. Grieser, *Rev. Chem. Eng.* **1999**, *15*, 41.
[23] K. Barbour, M. Ashokkumar, R. A. Caruso, F. Grieser, *J. Phys. Chem. B* **1999**, *103*, 9231.
[24] A. Gedanken, X. Tang, Y. Wang, N. Perkas, Y. Koltypin, M. V. Landau, L. Vradman, M. Herskowitz, *Chem. Eur. J.* **2001**, *7*, 4546.
[25] J. Zhang, J. Du, B. Han, Z. Liu, T. Jiang, Z. Zhang, *Angew. Chem. Int. Ed.* **2006**, *45*, 1116.
[26] M. Liu, P. Guyot-Sionnest, *J. Phys. Chem. B* **2005**, *109*, 22 192.
[27] W. Chen, *J. Colloid Interface Sci.* **2001**, *238*, 291.
[28] C. X. Kan, W. Cai, C. Li, L. Zhang, H. Hofmeister, *J. Phys. D* **2003**, *36*, 1609.
[29] G. H. Fu, W. P. Cai, C. X. Kan, C. C. Li, Q. Fang, *J. Phys. D* **2003**, *36*, 1382.
[30] C. Li, W. Cai, Y. Li, J. Hu, P. Liu, *J. Phys. Chem. B* **2006**, *110*, 1546.
[31] Y. Gao, L. Song, P. Jiang, L. F. Liu, X. Q. Yan, Z. P. Zhou, D. F. Liu, J. X. Wang, H. J. Yuan, Z. X. Zhang, X. W. Zhao, X. Y. Dou, W. Y. Zhou, G. Wang, S. S. Xie, H. Y. Chen, J. Q. Li, *J. Cryst. Growth* **2005**, *276*, 606.
[32] D. B. Williams, C. B. Carter, *Transmission Electron Microscopy*, Plenum Press, New York **1996**, p. 258.
[33] C. F. Bohren, D. R. Huffman, *Absorption and Scattering of Light by Small Particles*, Wiley, New York **1983**.
[34] J. D. Jackson, *Classical Electrodynamics*, Wiley, New York **1999**.
[35] F. J. García de Abajo, A. Howie, *Phys. Rev. Lett.* **1998**, *80*, 5180.
[36] F. J. García de Abajo, A. Howie, *Phys. Rev. B* **2002**, *65*, 115 418.
[37] B. T. Draine, P. J. Flatau, *J. Opt. Soc. Am. A* **1994**, *11*, 1491.
[38] The electromagnetic field can diverge near sharp corners separating continuous media. This is a mathematical pathology that is inherent to the assumption of local response and sharp boundaries. In the BEM, this is translated into divergences of the boundary sources near sharp corners that can cause numerical instability. In actual physical systems sharp corners do not exist (see Fig. 2), since atomic distances impose a discrete length of measure. Furthermore, the assumption of local response breaks down at non-physically small distances. By smoothing sharp corners through some rounding, these problems are solved and one finds a physical connection to the real particle behavior.
[39] T. Teranishi, M. Hosoe, T. Tanaka, M. Miyake, *J. Phys. Chem. B* **1999**, *103*, 3818.
[40] J. M. Petroski, Z. L. Wang, T. C. Green, M. A. El-Sayed, *J. Phys. Chem. B* **1998**, *102*, 3316.
[41] P. B. Johnson, R. W. Christy, *Phys. Rev. B* **1972**, *6*, 4370.

ADVANCED MATERIALS

Supporting Information

for

Advanced Materials, adma.200600475

Synthesis and Optical Properties of Gold Nanodecahedra with Size Control

Ana Sánchez-Iglesias[1], Isabel Pastoriza-Santos[1], Jorge Pérez-Juste[1], Benito Rodríguez-González[1], F. Javier García de Abajo[2], and Luis M. Liz-Marzán[1,*]

[1]Departamento de Química Física and Unidad Asociada CISC – Universidade de Vigo, 36310, Vigo, Spain, lmarzan@uvigo.es

[2]Centro Mixto CSIC-UPV/EHU and Donostia International Physics Center, Apartado 1072, 20080 San Sebastián, Spain

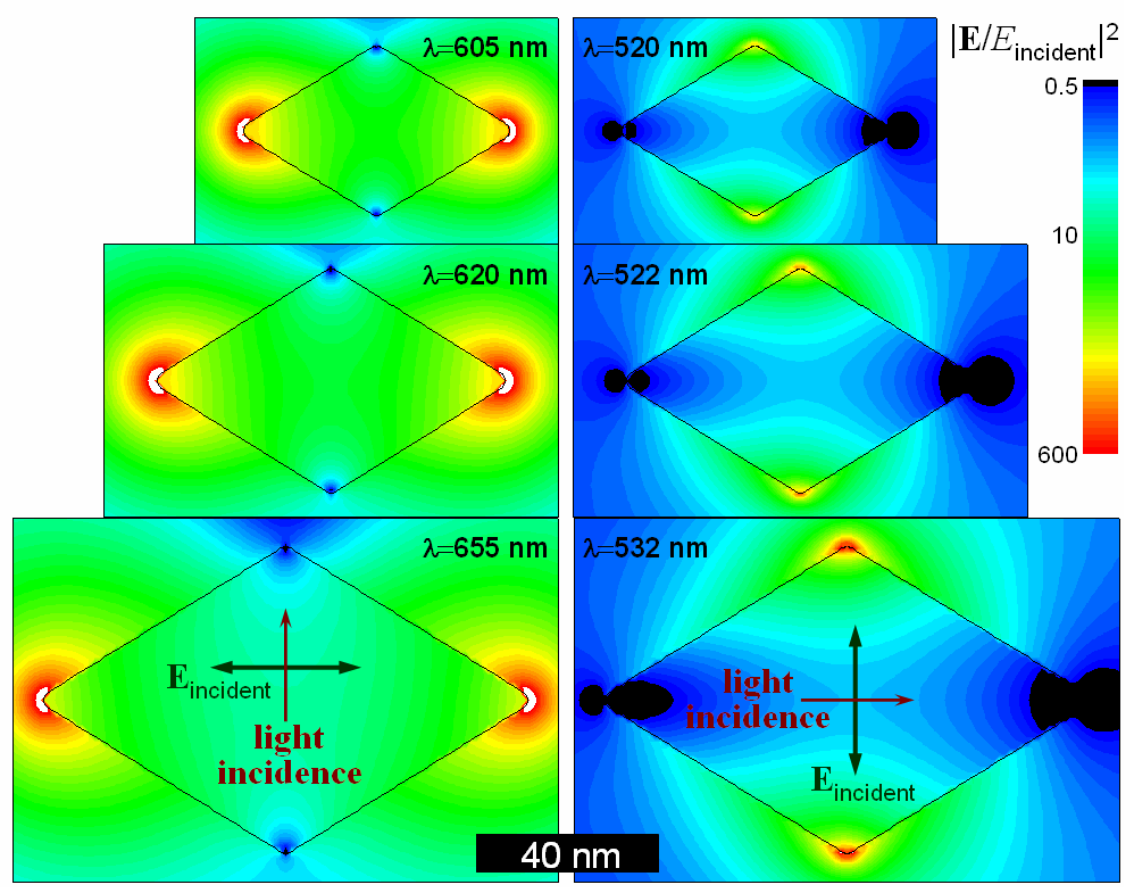

Figure S1. Plots of the calculated near field enhancement ($|E/E_{incident}|^2$) for bicones with three different dimensions (see Figure 4 in text) in the azimuthal (top, incident field along the horizontal symmetry plane) and polar (bottom, incident field along the symmetry axis) modes. Light is coming from below in the upper plot and from the left in the lower one, with the electric field contained in the plane of the plots. For the calculations, the corresponding wavelengths of maximum extinction cross section were used.

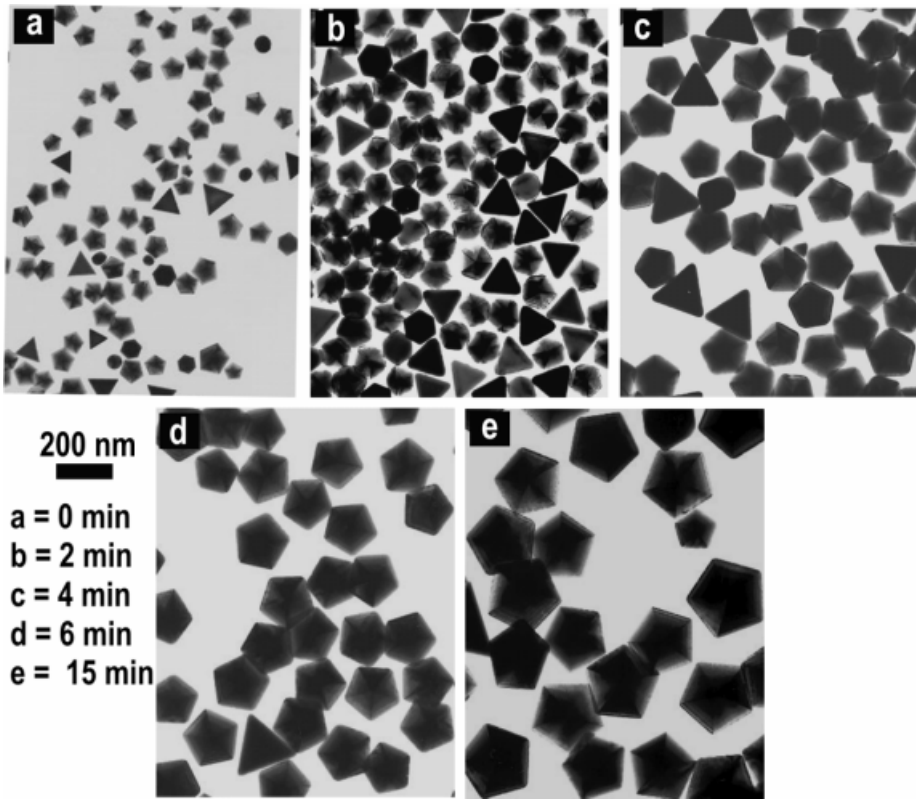

Figure S2. Transmission electron micrographs showing the growth process of preformed Au nanodecahedra (a) at different reaction times: 2min (b); 4 min (c); 6 min (d); 15 min (e).